



Photosynthetically Active Radiation, Attenuation Coefficient, Depth of the Euphotic Zone, and Water Turbidity in the Neva Estuary: Relationship with Environmental Factors

Mikhail Golubkov¹ · Sergey Golubkov¹

Received: 11 April 2022 / Revised: 19 December 2022 / Accepted: 20 December 2022 / Published online: 12 January 2023
© The Author(s), under exclusive licence to Coastal and Estuarine Research Federation 2023

Abstract

The coefficient of attenuation of photosynthetically active radiation ($K_d(\text{PAR})$) and the depth of the euphotic zone (Deu) are widely used to study biogeochemical processes and eutrophication in marine ecosystems. However, determination of $K_d(\text{PAR})$ and Deu in estuaries is hampered by the simultaneous influence of many environmental factors. In this study, we analyzed the relationship between water turbidity (Turb), $K_d(\text{PAR})$, Deu , and environmental variables in the Neva Estuary, the largest estuary in the Baltic Sea. The summer values of $K_d(\text{PAR})$ and Deu were significantly higher than in the open waters of the Baltic Sea and varied in the range of $0.5\text{--}9.1\text{ m}^{-1}$ and $0.5\text{--}8.5\text{ m}$, respectively. Mixed-effects regression analysis showed that the concentration of suspended mineral matter primarily determined the Turb . This variable fluctuated widely due to frequent wind-induced resuspension of bottom sediments and the periodic construction of port infrastructure in the shallow upper reaches of the estuary. Deu was determined by the depth of the water area, concentration of chlorophyll a , and concentrations of suspended mineral and organic matter. The average efficiency of using PAR energy for gross primary production (PP) was about 2%. However, PP did not depend on the amount of radiation incident on the water surface, but was mostly determined by underwater light and nutrient conditions. The study showed that more research on the impact of environmental variables on underwater light conditions in different regions is needed to predict the impact of climate change and anthropogenic factors on phytoplankton productivity in coastal areas.

Keywords Attenuation coefficient · Suspended matter · Chlorophyll · CDOM · Light conditions · Primary production · Baltic Sea

Introduction

Depth of euphotic zone (Deu) is one of the main parameters for calculating the value of primary production and cycles of nutrients in biogeochemical models of aquatic ecosystems, which model the primary productivity of phytoplankton (e.g., Behrenfeld and Falkowski 1997; Eilola et al. 2009; Neumann et al. 2015). It is defined as the layer of water that retains 1% of the amount of photosynthetically active radiation (PAR) that has reached the surface of the water. This

amount of PAR is sufficient for significant photosynthesis of autotrophic organisms (Kirk 2011). To find the depth of the euphotic zone, it is necessary to measure the intensity of PAR, which is the density of the flux of photons per second coming from the sun in the spectral range of 400–700 nm per unit of water surface, since aquatic autotrophs use light at these wavelengths for photosynthesis (Kirk 2011; Neumann et al. 2015). The decrease in PAR with depth is estimated using the vertical attenuation coefficient for downward irradiance ($K_d(\text{PAR})$). Knowing the Deu and $K_d(\text{PAR})$ values, supplemented by estimates of chlorophyll a concentration, is also important for evaluating the level of seawater eutrophication using remote sensing (Lee et al. 1996; Pierson et al. 2008; Kim et al. 2015; Alikas and Kratzer 2017; Kratzer et al. 2019; Gomes et al. 2020). For example, the $K_d(\text{PAR})$ value for the open waters of the Baltic Sea was calculated from satellite measurements of radiation at a wavelength of 490 nm ($K_d(490)$) in the top meter water layer, since

Communicated by Paul A. Montagna

✉ Mikhail Golubkov
golubkov_ms@mail.ru

¹ Zoological Institute of Russian Academy of Sciences, Universitetskaya Emb. 1, Saint Petersburg 199034, Russian Federation

this parameter is usually obtained from remote sensing (Pierson et al. 2008). In this study, a simple semi-analytical model was used to predict $K_d(490)$ and $K_d(\text{PAR})$. A series of model simulations based on variations in optically significant constituents over a range realistic for the Baltic Sea were used to define the relationship between these attenuation coefficients. Based on these model experiments, the coefficients of the equation for the dependence of $K_d(\text{PAR})$ on $K_d(490)$ were determined (Pierson et al. 2008).

PAR values at different depths are usually determined using scalar and planar quantum sensors (Arst et al. 2008; Kirk 2011). Scalar quantum sensors have a special spherical design, which gives possibility to detect radiation from all sides and take into account, among other things, photons reflected from various particles in the water or from the bottom. It measures the photosynthetic photon flux rate, called quantum scalar radiation (LI-COR 2022). Such sensors make it possible to determine in situ at what depth the PAR decreases to 1% of its value on the water surface. Unlike scalar quantum sensors, planar quantum sensors measure only the downwelling PAR; therefore, at a high concentration of light-scattering particles, they can significantly underestimate the PAR values (Arst et al. 2008).

$K_d(\text{PAR})$ can be calculated from measurements of the amount of incident radiation near the water surface and at different depths (Kirk 2011):

$$K_d(\text{PAR}) = -\frac{1}{d} \ln \frac{\text{PAR}_d}{\text{PAR}_0} \quad (1)$$

where PAR_0 and PAR_d are the PAR just below the surface and at depth d , respectively. The depth of the euphotic zone (Deu) is inversely proportional to $K_d(\text{PAR})$.

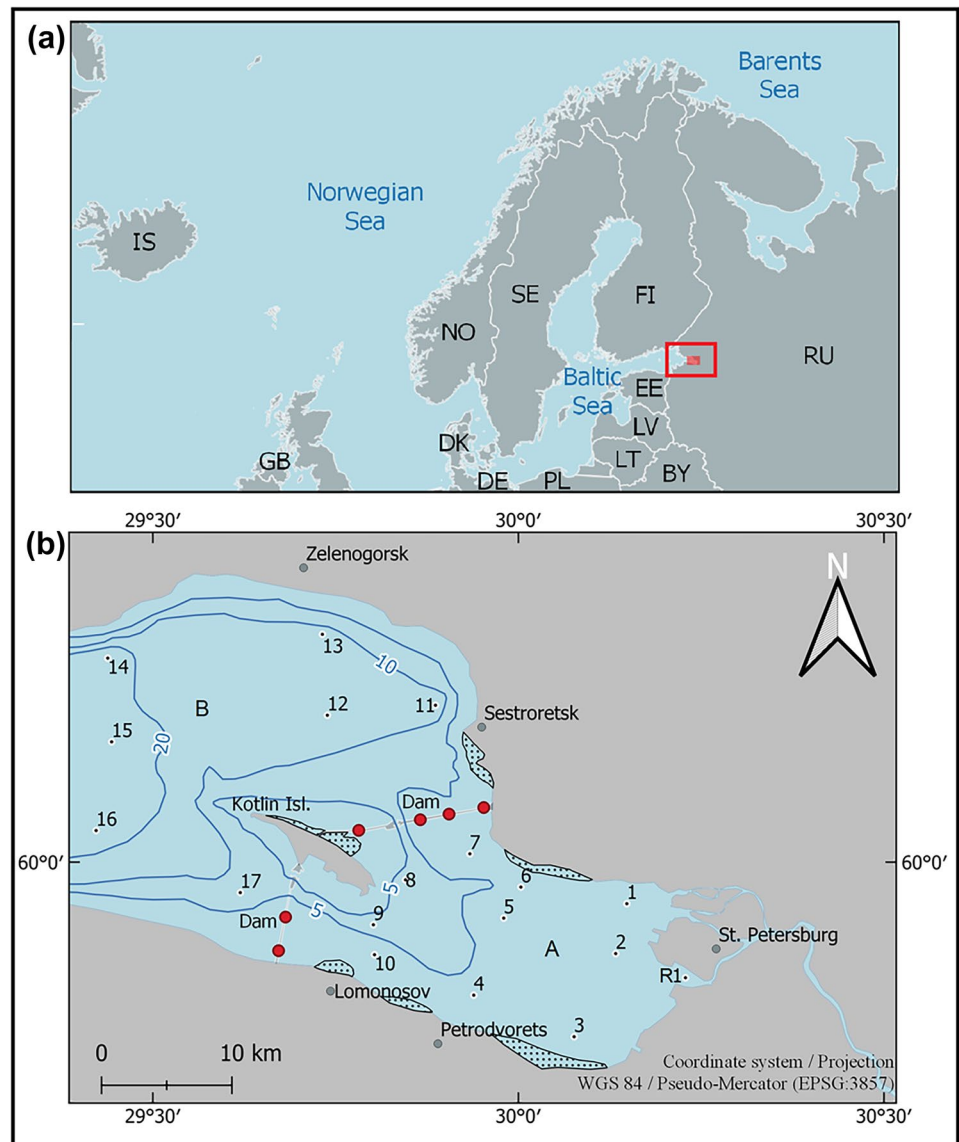
Factors responsible for changes in light conditions include suspended particulate inorganic and inanimate organic matter, phytoplankton, colored dissolved organic matter (CDOM), and water molecules. Their relative contribution to light attenuation and primary production (PP) limitation varies in space and time (Lund-Hansen 2004; Domingues et al. 2011; Thrane et al. 2014; Wang et al. 2019). For example, the attenuation of light with depth depends on the concentration of particulate organic and inorganic substances suspended in water (Armengol et al. 2003; Swift et al. 2006; Devlin et al. 2008). In estuaries and coastal lagoons, suspended particles can account for up to 75% of the PAR attenuation (McMahon et al. 1992; Philips et al. 1995; Christian and Sheng 2003). Coastal lagoons and shallow estuaries have high sediment surface area to water volume ratios and frequent wave resuspension of sediments. These features suggest that sediment resuspension, not increased pelagic productivity, often may be the dominant control on light availability in their waters (Armengol et al. 2003; Lawson et al. 2007; Devlin et al. 2008; Golubkov and

Golubkov 2022). On the other hand, a study of 75 boreal lakes showed that CDOM absorbed the largest fraction of PAR in the majority of lakes and phytoplankton pigments captured a minor fraction (Thrane et al. 2014). A particularly strong negative effect of CDOM on PP was observed at low concentrations of total phosphorus and photosynthetic pigments in water. Moreover, the degree of shading by these compounds is greatest in the blue part of the PAR spectrum (400–500 nm) that coincides with the absorption peak of chlorophylls and light-harvesting carotenoids (Thrane et al. 2014). The waters of the Baltic Sea have higher concentrations of CDOM compared to other marine and ocean areas (Kratzer and Moore 2018). There is also an opinion that CDOM has a significant impact on water transparency in regions with high river flow (Harvey et al. 2019).

It should also be taken into account that the contribution of various factors to the attenuation of PAR with depth varies on the spatial and temporal scales (Lund-Hansen 2004; Devlin et al. 2008; Wang et al. 2019). In different parts of the estuaries, the set of factors may differ depending on the depth, distance from the mouth of the river, the degree of water eutrophication, and weather conditions, which makes it more difficult to model phytoplankton productivity in coastal areas (Wang et al. 2019; Turner et al. 2021). The combined effect of various factors on light attenuation is also still poorly understood, which can sometimes reduce the effectiveness of measures to increase the depth of the euphotic zone in the estuary by reducing the nutrient load (Pedersen et al. 2014). Insufficient information on the degree of influence of specific factors on $K_d(\text{PAR})$ and Deu complicates the modeling of phytoplankton productivity in coastal areas. This problem is exacerbated due to climate change, which can lead to eutrophication of waters and an increase in the runoff of CDOM from the catchment in northern regions (Larsen et al. 2011; De Wit et al. 2016; Golubkov and Golubkov 2020; Golubkov 2021).

The Neva Estuary (Fig. 1), the largest estuary in the Baltic Sea, is located in the northeastern part of the sea. The Neva River is the most full-flowing river in the Baltic region with an average discharge of $2490 \text{ m}^3 \text{ s}^{-1}$ ($78.6 \text{ km}^3 \text{ year}^{-1}$) (Telesh et al. 2008). The catchment area of the estuary exceeds $280,000 \text{ km}^2$ (Golubkov and Golubkov 2020). It is located at the northern boundaries of the temperate zone and at the southern boundary of the subpolar zone (Meteoblue 2022). Climate type in the region according to Köppen-Geiger climate classification (Kottek et al. 2006) is Dfc—snowy climate, fully humid, with cool summers. The Neva Estuary is shallow and non-tidal and with a smooth salinity gradient from fresh water in the upper reaches (UR) to slightly saline in the middle reaches (MR) (Golubkov and Golubkov 2020). Temperature stratification is absent in the shallow UR of the estuary. The MR of the estuary is located between Kotlin Island and the

Fig. 1 The upper (A) and middle (B) reaches of the Neva Estuary with indication of sampling stations in midsummer 2012–2020. Lines: isobaths of 5, 10, and 20 m. Areas with dots indicate dense reeds. Dam is the St. Petersburg Flood Protection Facility. Red circles indicate water gates in the dam. Red rectangle in the top block of the map indicates location of the Neva Estuary. Two-letter country codes are given according to ISO 3166–1 alpha-2 (International Organization for Standardization 2022)



conditional boundary of $29^{\circ} 10' E$. In summer, constant temperature stratification is observed in this part of the estuary.

The ecosystem of the Neva Estuary is subject to strong anthropogenic impact, because the 5-million metropolis of St. Petersburg is located on its coasts (Golubkov et al. 2019a; Golubkov and Golubkov 2022). The Flood Protective Facility that consists of 11 dams has been separating the upper reaches (UR) of the estuary from its middle reaches (MR) since the end of 1980s (Fig. 1). Frequent wind-induced resuspension of bottom sediments in the upper shallow part of the estuary, as well as the periodic construction of new port facilities and the reclamation of new land, leads to a significant increase in the concentration of suspended matter in some parts of the estuary (Golubkov and Golubkov 2022). Its ecosystem is also subject to significant eutrophication due to high nutrient load and climate change, resulting

in increased biomass of phytoplankton, including harmful algae, and high primary production in the estuary (Golubkov and Golubkov 2021; Golubkov et al. 2019b, 2021). The concentration of chlorophyll *a* varied from 0.8 to 127 mg m^{-3} , and the gross primary production of plankton varied from 0.05 to $4.14 \text{ gC m}^{-2} \text{ day}^{-1}$ (Golubkov et al. 2017; 2021). The general ecological characteristics of the Neva Estuary and detailed description of both parts of the estuary were given earlier in Golubkov and Golubkov (2021).

The objective of this study was to determine the values of $K_d(\text{PAR})$ and Deu in the Neva Estuary. We also analyzed the relationships of environmental factors with their values. The assessment of the influence of various factors is important for clarifying the regional features of light attenuation when constructing biogeochemical models of water productivity and processing remote sensing data in the coastal zone of the Baltic Sea.

Materials and Methods

Data and Methods

To analyze the dependences of $K_d(\text{PAR})$ and Deu on environmental factors, we used data collected at sampling stations (Fig. 1) in late July–early August 2012–2020 during long-term scientific monitoring of the Neva Estuary ecosystem. Salinity (S) and temperature (T) were measured using a CTD90M probe from Sea & Sun Tech (Germany). The concentration of colored dissolved organic matter (CDOM) and chlorophyll a (CHL), as well as turbidity (Turb), was determined using Cyclop-7 sensors connected to a submersible C-6 multi-sensor platform (Turner Designs, USA). Cyclop-7 sensors checked and calibrated before measurements using Turner Designs solid standard. Cyclop-7 was additionally calibrated for CDOM according to the corrections proposed by Downing et al. (2012). Test material of humic substances (HS) from typical soils of the watershed of the Neva Estuary was obtained from the Department of Soil Science and Soil Ecology of St. Petersburg State University. HS solutions were prepared by dissolving 1 g of test material in 1 L organic-free deionized water, after which it was diluted to several solutions with HS concentration of 0.0005, 0.001, 0.002, 0.003, 0.004, 0.005, 0.007, and 0.01 mass percent. Fluorimeter measurements were made according to the method of Downing et al. (2012). The carbon concentration in these solutions was measured by high-temperature catalytic oxidation with Shimadzu TOC-L_{CPN/CSN} (Shimadzu Scientific Instrument, Japan) according to the method of Bird et al. (2003).

The PAR values were determined using a LiCOR-193SA scalar quantum sensor connected with a tripod to a CTD90M probe and controlled using Sea & Sun Tech software. LiCOR-193SA calibrated every 2 years (according to recommendations of manufacture) using spectrophotometer and reference silicon photodiodes that are traceable to the National Institute of Standards and Technology (NIST).

All probes were programmed to take readings at 1-s intervals. In order to minimize wave-related error, the readings were averaged over standard intervals in 10-cm increments. The value of PAR on the water surface (PAR_0) was taken as 100%, and the decrease in PAR with depth was expressed as a percentage of PAR_0 . The depth at which the PAR value reached 1% of the PAR_0 value was accepted as the depth of the euphotic zone (Deu). The number of photons reaching this depth (PAR_D) was also measured.

Total suspended particulate matter (SM), suspended particulate organic matter (SOM), and suspended particulate mineral matter (SMM) were considered environmental factors influencing Turb, $K_d(\text{PAR})$, and Deu . Water samples for determining SOM and SM were taken with a 2-L bathometer in the UR of the estuary: from the surface, at a depth

of half a meter above the bottom, and from three equidistant water layers between them. In the MR of the estuary, samples for determining SOM and SM were taken from water layers above the thermocline, which was determined using the CTD90M probe. Samples were taken from the surface, from a depth of 0.5 m above the thermocline and from three equidistant water layers between them. In this way, composite samples of 10 L were obtained. Half a liter of water was taken from these samples for laboratory determination of SOM and SM. SM concentration was determined after filtration through Whatman GF/F filters with a gravimetric technique (Grasshoff et al. 1999). The SOM concentration was determined by the dichromate acid oxidation of a suspension previously deposited on preheated (1 h, 105 °C) and preweighed GF/F filters (Grasshoff et al. 1999). The SMM concentration was determined by subtracting SOM from SM.

Statistical Analysis and Data Modeling

The Deu values were averaged for each station over the periods 2012–2020 and visualized using SURFER 8.0. Vertical PAR attenuation profiles in % were averaged for the river station (R1), separately for all stations in the UR of the estuary, and separately for all stations in the MR of the estuary. The results were visualized using Microsoft Excel. All data points were used for this (18 stations × 9 years = 162 numbers).

The indicator values at each station on each sampling date were used for correlation, regression, and mixed-effects regression analysis. Untransformed data were used for all statistical analysis. Data from stations where the PAR penetration depth was limited by the bottom were excluded from correlation, regression, and mixed-effects regression analyses. As a result, we used a matrix of 89 data points for the correlation-regression analysis (Table 1S). Correlation and linear regression analyses were performed using Microsoft Excel. The significance of the Pearson correlation coefficient was calculated taking into account the Bonferroni correction.

Part of the SOM data was missing in 2020; in this regard, we analyzed in mixed-effects regression analysis only data for 2012–2019. Some stations also did not have all indicators. As a result, for the mixed-effects regression analysis, we got a final matrix of 63 data lines for each indicator (Table 1S).

Linear mixed-effects models were performed to determine the most significant factors influencing Deu and Turb using function “lme” from package “lme4” (Bates et al. 2015) of the R software (version 4.2.1) (R Core Team 2022). The null models with no fixed effects except for an intercept were built separately for Turb and Deu . The full models with all environmental indices were also built separately for Turb and Deu . The script was the same as described by Winter (2013) in “Part 2: A very basic tutorial for performing linear mixed effects analyses.” Then, the function “dredge” from

R package “MuMIn” (Barton 2022) was used to find best mixed models for Deu and Turb. As a result, we performed two multiregression models with random effects for Turb and for Deu. The residual plots were checked for all final models and it showed that the residuals were unbiased and homoscedastic. In this way, combinations of factors most strongly influencing separately Turb and Deu were found.

To evaluate the significance of the obtained models with a random factor, we ran the “r.squaredGLMM” command from the “MuMIn” package and found that Adj R^2 for models without a random factor (R^2_m) was lower than for models with a random factor ($R^2_c = 0.77$). Marginal R^2_m represents the variance explained by the fixed effects. Conditional R^2_c is interpreted as a variance explained by the entire model, including both fixed and random effects (Barton 2022). Accordingly, mixed-factor models better described the original data. After that, we ran the “ranova” function from the R package “lmerTest” (Kuznetsova et al. 2017) and checked the significance of random effects. We also used the “anova” function from the R package “lmerTest” package to run the type III analysis of variance with Satterthwaite’s method and test the significance of the predictors (fixed effects). In addition, using the “anova” command from the “lmerTest” package, we compared our mixed models with random null models separately for Turb and Zeu in a likelihood ratio test, as suggested by Winter (2013). As a result, we got the AIC, chi-square value, probability of chi-square value, and log-likelihood values. The last function calculates the log-likelihood for some parameter values, given a random sample and distribution. This allowed us to conclude that the models we obtained describe the initial data well (better than random models with all factors). The full results of the final models are presented in Tables 2S and 3S.

Transfer Efficiency of PAR to Gross Primary Production of Plankton

Using our data on the gross primary production of plankton in the Neva Estuary published earlier (Golubkov and Golubkov 2021) and the data of this study, we calculated the transfer efficiency of photosynthetically active radiation on the water surface (PAR_0) to gross primary production of plankton. We performed the calculation in the same way as O’Gorman et al. (2016). The values of gross primary production were expressed in $gC\ m^{-2}\ day^{-1}$. The conversion factor for PAR that was used in the calculations was $1\ mol\ photon\ m^{-2}\ day^{-1} = 6.13\ g\ C\ m^{-2}\ day^{-1}$ by relating the Q/W ratio $2.5 \times 10^{21}\ photon\ s^{-1}\ kJ^{-1} = 4.15 \times 10^{-3}\ mol\ photon\ kJ^{-1}$ (Morel and Smith 1974) with the reciprocal of the energy content of glucose expressed in carbon units $15.7\ kJ\ g^{-1}\ glucose = 25.4 \times 10^{-3}\ g\ C\ kJ^{-1}$ (Southgate and Durnin 1970).

Results

The Attenuation Coefficient of Photosynthetically Active Radiation and the Depth of the Euphotic Zone

The number of photons at different stations, determined just below the water surface, changed by almost two orders of magnitude during the study period, averaging $22.98\ mol\ m^{-2}\ day^{-1}$ (Table 1). At the same time, the PAR attenuation coefficient and the depth of the euphotic zone at different stations changed 17 times.

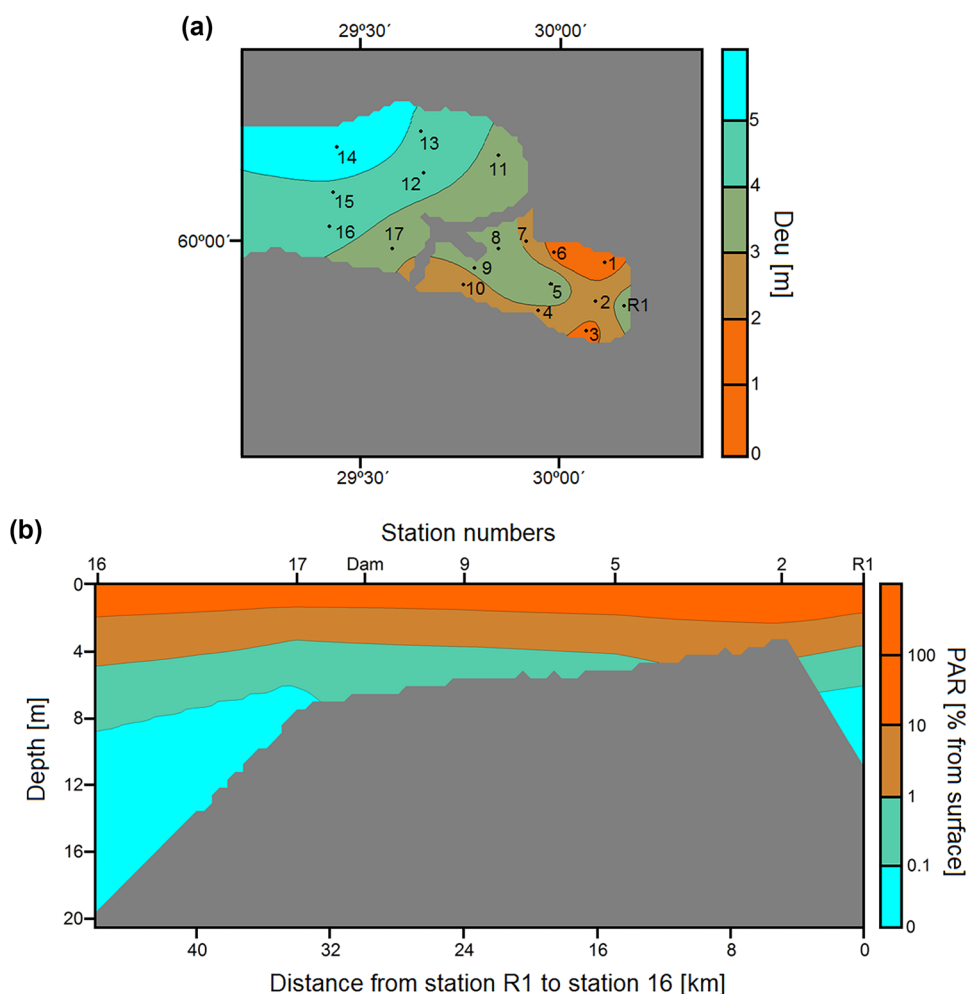
The minimum Deu value of 0.5 m was in 2020 at station 6 located in the UR of the estuary, and the maximum value was 8.5 m at station 14 in 2016 in the MR of the estuary. The spatial distribution of this indicator showed the lowest Deu values in the upper and coastal parts of the estuary (Fig. 2a). In addition, the euphotic zone was deeper at the confluence of the Neva River than downstream in the estuary. Farther from the mouth of the river, Deu first decreased slightly, and then began to increase and reached its highest values in the northwestern part of the MR (Fig. 2b). Such a spatial distribution of Deu is associated not only with optical characteristics, but with water depth in various parts of the estuary. For example, on average, 4% of the PAR falling on the water surface reached the bottom at station 2 (Fig. 2b). However, on one of the dates, 21% of the surface PAR reached the bottom at this station. At other stations in the UR of the estuary, more than 1% of the PAR also periodically reached the bottom. The depth of the euphotic zone was always limited by the bottom at stations 1 and 2 and usually at stations 3, 4, and 6 in the UR of the estuary (Fig. 2a). On the contrary, less than 1% of the PAR always reached the bottom at river station R1 (depth 11 m) and at all stations in the MR of the estuary (Fig. 2a, b).

PAR attenuation profiles averaged over 2012–2020 showed that the profiles for the UR and MR of the estuary almost coincided (Fig. 3). The depth at which 10% of PAR remained from its values on the water surface differed slightly and averaged 1.5 m, 1.65 m, and 1.7 m in the river and in the upper and middle reaches of the estuary,

Table 1 Euphotic zone depth (Deu), quantum scalar PAR just below the water surface (PAR_0) (zero point of the Deu profile), and average PAR attenuation coefficient for the euphotic zone ($K_d(PAR_{Deu})$) in the upper and middle reaches of the Neva Estuary at the end of July to early August 2012–2020

	Min	Max	Average	Median
$PAR_0, mol\ m^{-2}\ day^{-1}$	1.21	101.41	22.98	13.95
$K_d(PAR_{Deu}), m^{-1}$	0.54	9.21	1.65	1.40
Deu, m	0.5	8.5	3.4	3.3

Fig. 2 The average depth of the euphotic zone **(a)** and the vertical distribution of PAR **(b)** in the upper and middle reaches of the Neva Estuary in late July–early August 2012–2020. The depth of the euphotic zone was always limited by the bottom at stations 1 and 2 and usually at stations 3, 4, and 6. Dam is the St. Petersburg Flood Protection Facility



respectively. Therefore, on average, the PAR attenuation with depth occurred a little faster in the Neva River (Fig. 3a) than in both reaches of its estuary (Fig. 3b, c). Another difference was that the spread of standard deviations was higher in the shallow UR than in the deep MR of the estuary (Fig. 3b, c). In addition, the spread of standard deviations of PAR attenuation in the water column in the Neva River was less than in the estuary, especially at depths more than 2 m (Fig. 3a).

In the Neva Estuary, the power-law relationship between the Deu and the $K_d(\text{PAR})$ gave a high coefficient of determination (Fig. 4). The depth of the euphotic zone up to the value of $K_d(\text{PAR}_{\text{Deu}}) \sim 2$ decreased significantly as it increased. However, at $K_d(\text{PAR}_{\text{Deu}}) > 2$, the Deu values remained almost unchanged (Fig. 4). The resulting power regression is described by the formula:

$$\text{Deu} = 4.6052K_d(\text{PAR}_{\text{Deu}})^{-1} \tag{2}$$

Environmental Factors Affecting the PAR Attenuation Coefficient and the Depth of the Euphotic Zone

The minimum, maximum, average, and median values of the environmental indicators used in the statistical analysis are shown in Table 2.

An analysis of Pearson’s pair correlations showed that all optical characteristics of water correlated with each other. $K_d(\text{PAR}_{\text{Deu}})$ was negatively correlated with Deu, i.e., with an increase in the PAR attenuation coefficient, the depth of light penetration into the water column decreased (Table 3).

Vertical attenuation coefficient of PAR correlated positively with water turbidity, concentrations of total suspended particulate matter, and mineral suspended particulate matter, as well as with the percentage of the mineral fraction in the total suspended matter. It correlated negatively with depth,

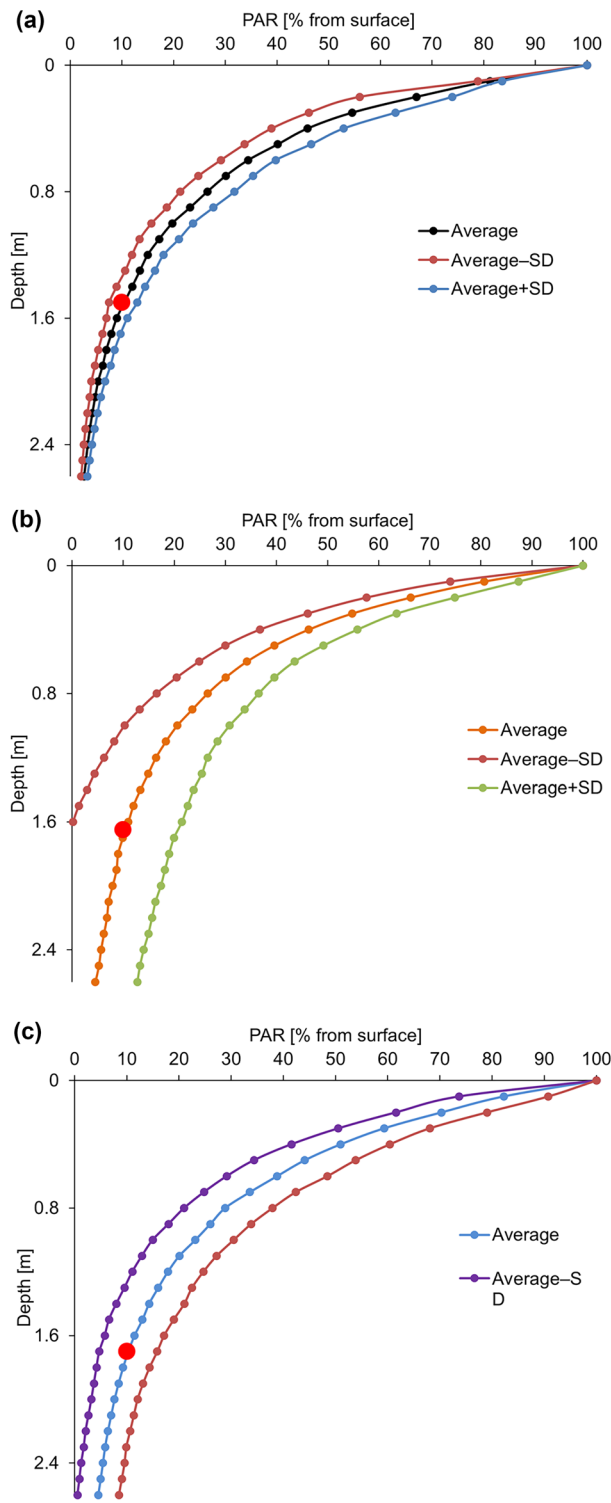


Fig. 3 Average, average minus, and average plus standard deviation vertical profiles of PAR attenuation in the Neva River (a) and in the upper (b) and middle reaches (c) of the Neva Estuary during the study period of 2012–2020. The red dots mark the depth at which, on average, 10% of PAR remained of its values on the water surface. This depth averaged 1.5 m, 1.65 m, and 1.7 m in the river, in the upper and middle reaches of the estuary, respectively

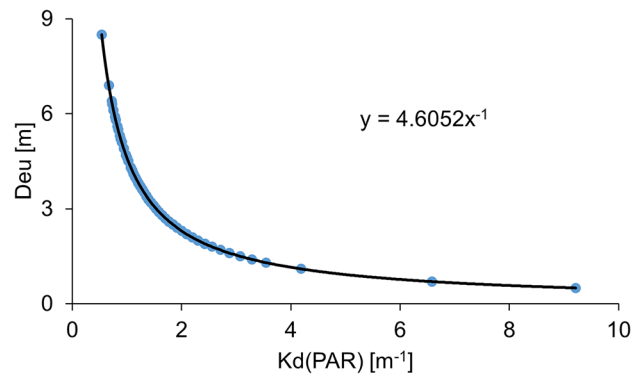


Fig. 4 Dependence of the depth of the euphotic zone (Deu) on the PAR attenuation coefficient ($K_d(\text{PAR}_{\text{Deu}})$) in the Neva Estuary in late July–early August 2012–2020

water salinity, percentage of organic suspended matter, and chlorophyll *a* in the total suspended matter. Water turbidity, in turn, was negatively correlated with *D*, *S*, SOM%, and CHLm% (Table 3). However, water salinity was apparently important not in itself, but as a measure of distance from the river mouth, since the water turbidity decreased at deeper and more seaward stations. Water turbidity positively correlated with values of SM, SMM, and SMM% (Table 3). The euphotic zone depth correlated negatively with Turb, SM, SMM, and SMM% and positively with *D*, *S*, SOM%,

Table 2 Morphometric, physio-chemical, and biological indicators at sampling stations in the Neva Estuary during the period of 2012–2020. *D*, water depth (m); *D*_{11–17}, water depth at stations 11–17 (m); *DT*_{11–17}, thermocline depth at stations 11–17 (m); *S*, salinity (PSU); *Turb*, turbidity (NTU); *CDOM*, colored dissolved organic matter (g m^{-3}); *SM*, suspended particulate matter (g m^{-3}); *SOM*, suspended particulate organic matter (g m^{-3}); *SMM*, suspended particulate mineral matter (g m^{-3}); *CHL*, chlorophyll *a* (mg m^{-3}); *SOM%*, percent SOM in SM; *SMM%*, percent SMM in SM; *CHLm%*, percent CHL in SM; *CHLom%*, percent CHL in SOM

	Min	Max	Average	Median
<i>D</i>	2.5	25.5	11.6	10.4
<i>D</i> _{11–17}	6.5	25.5	14.9	13.0
<i>DT</i> _{11–17}	2.1	19.2	8.2	7.2
<i>S</i>	0.06	2.24	0.51	0.38
<i>Turb</i>	2.28	65.68	8.61	5.61
<i>CDOM</i>	10.82	21.05	14.07	13.56
<i>SM</i>	2.53	22.60	5.93	4.57
<i>SOM</i>	1.10	6.66	2.53	2.45
<i>SMM</i>	0.21	20.15	3.40	1.92
<i>SOM%</i>	9.12	94.91	53.38	55.13
<i>SMM%</i>	5.09	90.88	46.62	44.87
<i>CHL</i>	8.82	85.47	20.42	15.81
<i>CHLm%</i>	0.04	1.45	0.42	0.41
<i>CHLom%</i>	0.04	2.10	0.88	0.80

Table 3 Pearson’s correlation coefficients. Only statistically significant correlations (p -value < 0.01) are shown, taking into account the Bonferroni correction. *ns*, not significant. Abbreviations are the same as in Tables 1 and 2

	Deu	Kd(PAR _{Deu})	Turb	CHL
Kd(PAR _{Deu})	-0.83			
Turb	-0.63	0.88		
CHL	ns	ns	ns	
PAR ₀	ns	ns	ns	ns
PAR _D	ns	ns	ns	ns
<i>D</i>	0.57	-0.44	ns	ns
<i>S</i>	0.56	ns	ns	ns
CDOM	ns	ns	ns	ns
SM	-0.55	0.85	0.95	ns
SOM	ns	ns	ns	ns
SMM	-0.55	0.84	0.96	ns
SOM%	0.53	-0.55	-0.57	ns
SMM%	-0.53	0.55	0.57	ns
CHLom%	ns	ns	ns	0.61
CHLm%	ns	ns	-0.40	0.48

and CHLm%. The highest and most significant correlation for Deu was with water turbidity (Table 3). The depth of the euphotic zone depended with a high degree of confidence on the turbidity (Fig. 5). Accordingly, the depth of the euphotic zone in the midsummer in the Neva Estuary can be calculated from the water turbidity using the formula:

$$\text{Deu [m]} = 7.48\text{Turb}^{-0.40}[\text{NTU}] \tag{3}$$

Although the correlation coefficient between Turb and Deu was very high, it was lower than one (Fig. 5). Accordingly, it can be assumed that the set of factors influencing these indicators was different. We performed mixed-effects regression analysis using a mixed model for Turb and Deu, which allowed us to obtain statistically significant linear mixed-effects models for both indicators (Table 4).

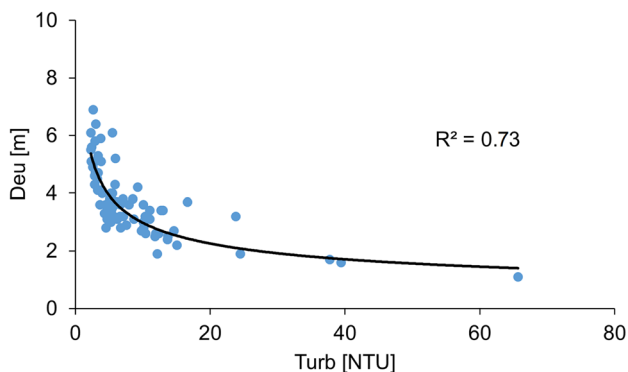


Fig. 5 Relationship between of the euphotic zone depth (Deu) and the water turbidity (Turb) in the Neva Estuary

A mixed-effects model for water turbidity in the estuary with three predictors gave the most accurate results. The predictors were the depth of the water area (*D*), the concentration of suspended particulate mineral (SMM), and suspended particulate organic matter (SOM). This model corresponds to the regression equation:

$$\text{Turb [NTU]} = 4.83 + 0.87\text{SMM}[\text{gm}^{-3}] + 0.48\text{SOM}[\text{gm}^{-3}] - 0.15\text{D}[\text{m}] \tag{4}$$

The water turbidity was affected to the greatest extent by SMM, which explained 91% of the variance; second and third places were taken by *D* and SOM, which together explained 9% of the variance (Table 5). Although the second and third predictor, *D* and SOM, improved the reliability of the model, they were important only in combination with the first predictor.

The mixed-effects model showed that the depth of the euphotic zone in the Neva Estuary depended on a combination of four environmental factors: the depth of the water area, the concentration of chlorophyll *a*, and the concentrations of suspended particulate mineral and organic matter (Eq. 5).

$$\text{Deu [m]} = 3.95 + 0.08\text{D}[\text{m}] - 0.02\text{Chl}[\text{mgm}^{-3}] - 0.06\text{SMM}[\text{gm}^{-3}] + 0.13\text{SOM}[\text{gm}^{-3}] \tag{5}$$

Analysis of variance showed that the main predictor of the model was water depth, which explained 60% of the variance. Chlorophyll *a* concentration, which explained 26% of the variance, was the second most important predictor (Table 5). The remaining two predictors were not statistically significant, but together, they explained 14% of the variance (Table 5).

Analysis of random effects showed that there were no statistically significant random effects on the turbidity model (Table 6). At the same time, “Year” (the year, when samples were taken) had a statistically significant random effect on the Deu model.

Mixed-effects regression analysis also showed that, although Turb and Deu in the Neva Estuary were closely and significantly related, the sets of factors affecting these two indicators in the estuary were somewhat different. The turbidity of water was almost completely determined by the concentration of SMM. The depth of the euphotic zone according the result of mixed-effects regression analysis was determined by a large number of factors, and two of them, the depth of the water area and the concentration of chlorophyll, were statistically significant. An unexpected result was that the concentration of CDOM, varying within the study area by 2 times (Table 2), did not show significant correlations in the analysis of pairwise correlations (Table 3), and was not a predictor in mixed-effects regression models for Turb and Deu (Table 5).

Table 4 The results of comparing the obtained mixed models with null models using the Likelihood Ratio Test. *Df*, degree of freedom; *AIC*, Akaike information criterion; *logLik*, log-likelihood; *Chisq*, chi-square value; *Pr(> Chisq)*, probability; *R²m*, marginal *R²*; *R²c*, conditional *R²*

	Df	AIC	logLik	Chisq	Df	Pr(> Chisq)	R ² m	R ² c
Turb.null	4	320.8	−156.4					
Turb.model	7	276.9	−131.5	49.97	3	<0.001	0.74	0.84
Deu.null	4	167.6	−79.8					
Deu.model	8	162.1	−73.0	13.5	4	0.009	0.51	0.75

Diagrams of the horizontal distribution of the euphotic zone depth, constructed according to empirical data (Fig. 2a) and according to mixed-effects regression equation (Fig. 6), are almost identical. Therefore, the resulting multiple regression equation is consistent with these data.

Transfer Efficiency of PAR to Gross Primary Production of Plankton

The transfer efficiency of photosynthetically active radiation on the water surface (PAR₀) to gross primary production of plankton in the Neva Estuary was 1.91%. The utilization efficiency of PAR in the estuary decreased with an increase in its intensity on the water surface (Fig. 7a), because the primary production of plankton did not depend on PAR₀ (Fig. 7b).

Discussion

Summer Kd(PAR) values in the Neva Estuary (Table 1) were significantly higher compared to Kd(PAR) values in the open sea waters of Northern Europe. For example, Kd(PAR) value was about 0.4 m^{−1} in the open waters of the North Sea (Riegmann and Colijn 1991). In the study covering the north of the Gulf of Bothnia, the western part of the Gulf of Finland, and the central and southern parts of the Baltic Sea to the Danish Straits, its values varied from 0.10 to 0.95 m^{−1} (Neumann et al. 2015). In the Danish Straits

connecting Baltic and North Seas, Kd(PAR) varied within 0.1–0.6 m^{−1} in different seasons (Lund-Hansen 2004). In these straits, the depth of the euphotic zone was 8.3 m, and Kd(PAR) was 0.56 m^{−1} in March during the peak of spring bloom. In June, Deu was 15.7 m and Kd(PAR) decreased to 0.29 m^{−1} (Lund-Hansen 2004). In the Neva Estuary, with a minimum Kd(PAR) of 0.54 m^{−1}, the maximum depth of the euphotic zone was 8.5 m (Table 1), which practically coincides with the minimum Deu in the Danish Straits. In these straits, 50% of PAR was attenuated at depths of 1.6 and 2.4 m, when Kd(PAR) were 0.56 and 0.29 m^{−1}, respectively (Lund-Hansen 2004). For comparison, in the Neva Estuary, PAR decreased to 50% at a depth of about 0.4–0.5 m at the peak of summer bloom (Fig. 3), and the maximum Kd(PAR) was more than 9.0 m^{−1} (Table 1).

The values of Kd(PAR) and Deu in the Neva Estuary are close to the values of these indicators in the lakes located in the watershed of the Gulf of Finland. A study of Finnish lakes located on the northern coast of the Gulf of Finland showed that Kd(PAR) in these lakes varied within 1.7–3.5 m^{−1} in summer (Jones and Arvola 1984). In the lakes located on the southern coast of the Gulf of Finland, the Kd(PAR) values varied closer to the range in the Neva Estuary than in the Finnish lakes. For example, Kd(PAR) was between 0.7 and 2.5 m^{−1} in the mesotrophic Lake Pepsi with an average depth of 7 m (Nõges 2001). In the shallower eutrophic Lake Vortsjarvi (average depth 2.8 m), Kd(PAR) varied from 1.65 to 3.40 m^{−1} (Arst 2003). In the hypereutrophic and shallowest lake Harku (maximum depth 2 m), Kd(PAR) ranged from 2.5 to 7.7 m^{−1} (Arst et al. 2008). These values were similar to

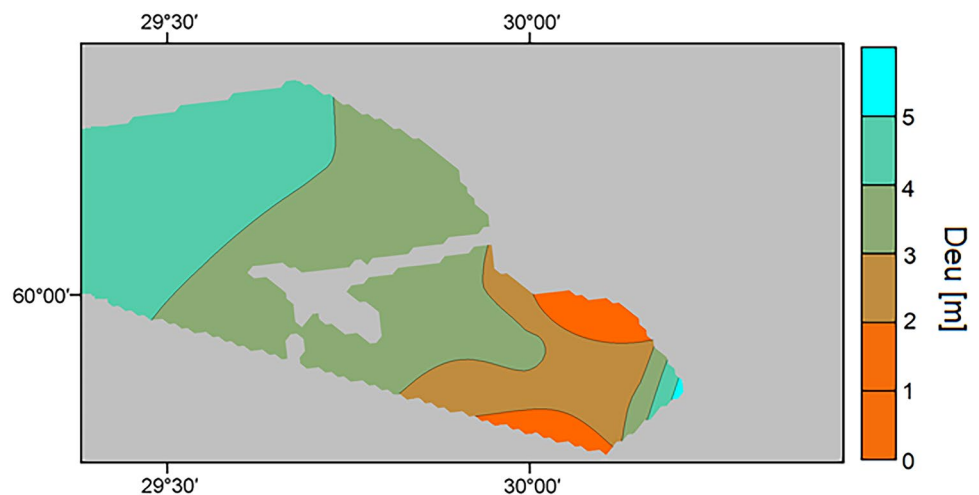
Table 5 Analysis of variance for model predictors. *F*, *F* value; *p*-value, probability of *F* value. Abbreviations are the same as in Tables 1 and 2. Bold font indicates statistically significant predictors

<i>Y</i> variables	<i>X</i> variables	<i>F</i>	<i>p</i> -value	Contribution to model variance (%)
Turb	SMM	77.8	<0.001	91
	<i>D</i>	5.02	0.053	6
	SOM	2.62	0.113	3
Deu	<i>D</i>	18.80	<0.001	60
	Chl	8.27	0.006	26
	SMM	3.18	0.081	10
	SOM	1.34	0.252	4

Table 6 ANOVA-like table with test of random-effect terms in the model. Abbreviations are the same as in Tables 1 and 4. *LRT*, likelihood ratio test value

<i>Y</i> variables	<i>X</i> variables	logLik	AIC	LRT	Pr(> Chisq)
Turb	none	−131.44	276.9		
	Station	−132.73	277.5	2.582	0.1080
	Year	−131.60	275.2	0.309	0.5781
Deu	none	−73.04	162.08		
	Station	−74.10	162.21	2.130	0.14445
	Year	−78.43	170.86	10.787	0.00102

Fig. 6 The euphotic zone depth (Deu) in the Neva Estuary calculated by Eq. 5



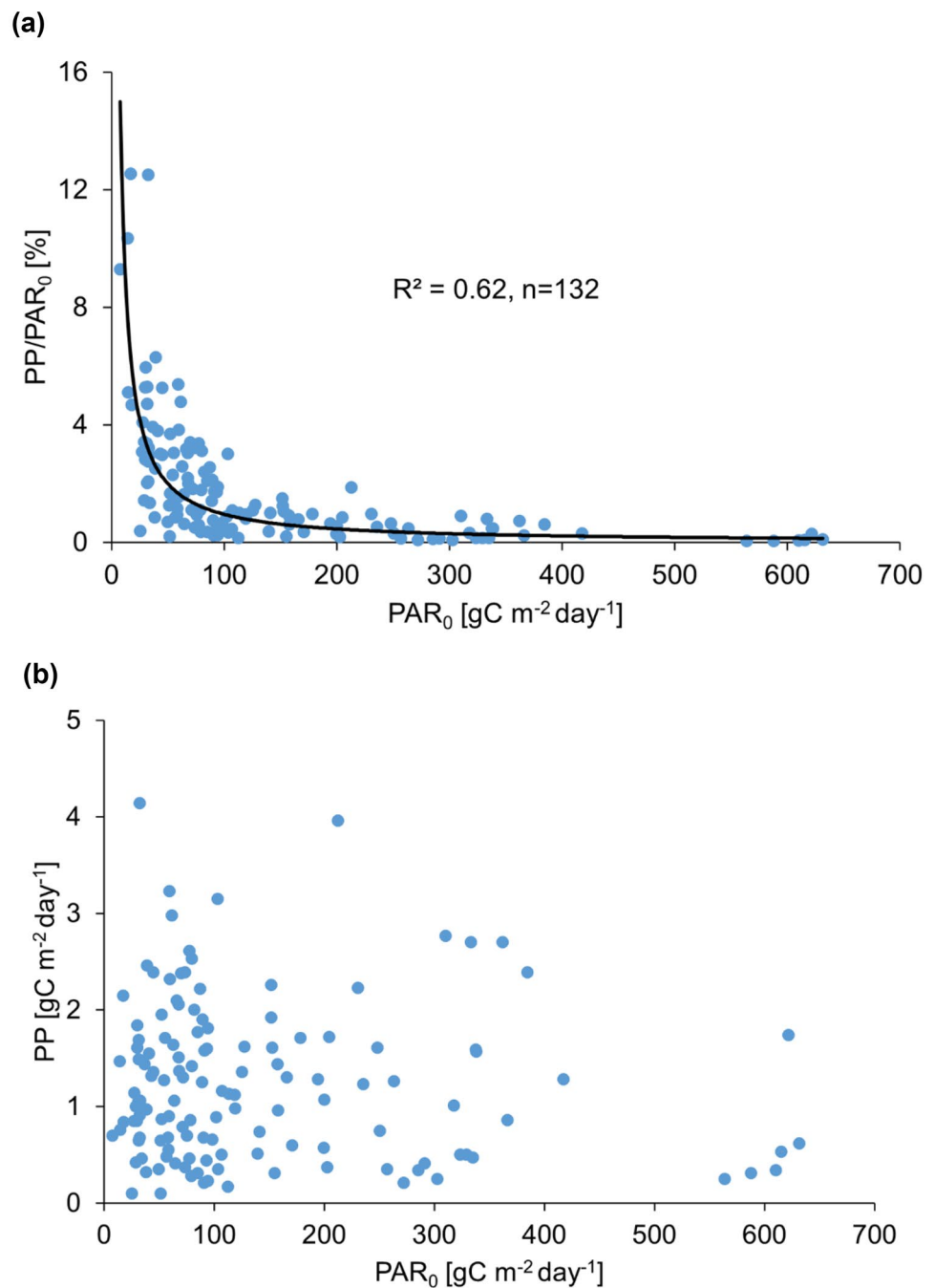
$K_d(\text{PAR})$ values ($0.5\text{--}9.2\text{ m}^{-1}$) in the Neva Estuary. Therefore, the values of $K_d(\text{PAR})$ and the depth of the euphotic zone in the Neva Estuary and other coastal shallow areas of the Baltic Sea were more similar to their values in the lakes located on the catchment area of the Gulf of Finland than to the waters of the open part of the Baltic Sea.

The main factors affecting the values of $K_d(\text{PAR})$ and Deu are usually considered to be the concentrations of SM and CDOM. It has also been shown that SM and CDOM primarily filter out the short-wavelength part of the spectrum, while the long-wavelength of PAR goes deeper (Kirk 2011; Chupakova et al. 2018; Zhang et al. 2020). Changes in the concentration of SM, including non-living organic matter and phytoplankton, explained up to 85% of the variability in water transparency even in the open part of the Baltic Sea (Baltic Proper) (Kratzer and Tett 2009; Harvey et al. 2019). In the Danish Straits, changes in $K_d(\text{PAR})$ were 42% dependent on SM, 32% on phytoplankton biomass, and 17% on CDOM (Lund-Hansen 2004). According to our data, the mineral and organic fractions of suspended particulate matter, as well as phytoplankton biomass, which was measured by the concentration of chlorophyll a , were also predictors of the depth of the euphotic zone in the Neva Estuary (Table 5). It should be taken into account that in the shallow UR of the estuary, a high concentration of suspended matter is mainly observed due to the resuspension of bottom sediments in windy weather (Martyanov and Ryabchenko 2016), or as a result of the construction of port infrastructure, which is periodically renewed in the UR of the estuary (Ryabchuk et al. 2017; Golubkov and Golubkov 2022). During these periods, the concentration of SM reached 180 g m^{-3} and it mainly consists of SMM, the content of which in SM can exceed 90% (Golubkov and Golubkov 2022). The depth of the euphotic zone during such periods averaged about 1.5 m in the UR of the estuary (curve of average +SD PAR in Fig. 3b). On the contrary, in calm weather during the period when the construction of ports was not carried out, the

concentration of SM in the water in the UR of the estuary significantly decreased, and the PAR values decreased with depth much more slowly (curve of average–SD PAR in Fig. 3b). In contrast to the UR, there was no resuspension of bottom sediments due to wind mixing in the stratified MR of the estuary (the thermocline depth is less than the depth of the water area, Table 2). In this part of the estuary, the PAR values at different depths varied mainly due to the inflow of some SM from the UR of the estuary or periodic weather-related algal blooms occurring there (Golubkov and Golubkov 2020, 2021). As a result, the variation in PAR values at different depths in the MR of the estuary was less than in its UR (Fig. 3b, c). At the same time, the differences in the average vertical profiles of PAR attenuation with depth between the upper and middle reaches of the Neva Estuary were not so significant. The shallow depths of the euphotic zone in the upper reaches of the estuary were often determined by its shallowness, when the lower part of the PAR attenuation profile was “cut off” by the bottom (Fig. 2b).

Resuspension of bottom sediments both in windy weather and due to the construction of port infrastructure in the Neva Estuary led to a multiple increase in the concentration of suspended mineral matter (SMM) and a decrease in the proportion of organic matter (SOM%) and the proportion of chlorophyll (CHLm%) in suspended matter (SM). As a result, turbidity was positively and euphotic zone depth was negatively correlated with SM and SMM, and vice versa, Turb was negatively correlated, while Deu was positively correlated with SOM% and CHLm% (Table 3). The short-term resuspension of bottom sediments due to strong wind apparently did not have a subversive effect on phytoplankton, since it corresponded to the natural dynamics of the estuary ecosystem. However, a long-term increase in the concentration of suspended matter during the construction of port infrastructure resulted in a significant decrease in primary production of plankton (Golubkov and Golubkov 2022).

Fig. 7 Dependence of transfer efficiencies of PAR energy at the water surface (PAR_0) to first trophic level (a) and primary production (PP) on PAR_0 (b) in the Neva Estuary in midsummer 2012–2020



CDOM concentration is an important parameter in Deu calculations in hydrodynamic-biogeochemical models for open and coastal areas of the Baltic Sea (Savchuk 2002), especially for its northern parts, such as the Gulf of Bothnia (Savchuk 2002; Neumann et al. 2015; Harvey et al. 2019). For example, water transparency in the coastal zone of the Swedish part of the Gulf of Bothnia significantly depended on the concentration of CDOM (Harvey et al. 2019). Our studies also showed high concentrations of CDOM in the upper and middle reaches of the Neva Estuary (Table 2) that were even slightly higher than in the coastal zone of the Gulf

of Bothnia. These high concentrations were due to a very large catchment area of the Neva River, covering 281,000 km² (Telesh et al. 2008), which has many swamps. However, changes in CDOM concentration were not a predictor in mixed-effects regression models for Deu in the upper and middle reaches of the Neva Estuary (Table 5). The reason for this, apparently, was that its concentration in different parts of the UR and MR of the estuary changed only 2 times during the summer period (Table 2). In opposite, according to our data, the concentration of SM in different parts of the estuary altered by 9 times (Table 2). The maximum

SM values were observed in the shallow parts of the estuary, and the minimum values were in its deep parts. For this reason, water depth and the concentration of SM were one of the main predictors in mixed-effects regression equation for Deu and showed significant pairwise correlations with Deu and Kd(PAR) in the Neva Estuary (Tables 3, 5). Therefore, depth may be also a good predictor for the depth of the euphotic zone in shallow coastal waters of the Baltic Sea. A similar conclusion was made for water transparency in the East Japan and East China seas, where the depth of coastal waters identified as an important predictor of this indicator (Kim et al. 2015). At the same time, depth was not taken into account in the biogeochemical models developed for the Baltic Sea, since the bulk of the data for their calibration was obtained in open Baltic waters, where depth is not important (Savchuk 2002; Neumann et al. 2015; Harvey et al. 2019; Kratzer et al. 2019). This limits the applicability of these models to the shallow coastal areas of the Baltic Sea.

A more significant effect of CDOM on Deu in open waters compared to coastal waters can be also explained by a faster decrease in the concentration of suspended matter due to its sedimentation compared to the concentration of dissolved substances with distance from the river mouth (Lizitzin 1999; Emelianov 2003; Bianchi 2007; Shirokova et al. 2017). As a result, the role of CDOM in PAR attenuation can increase with distance from the river mouth even if their concentration does not change (Pedersen et al. 2014). However, in the shallow Neva Estuary with frequent resuspension of bottom sediments and high level of eutrophication, this parameter was insignificant as compared with SMM, SOM, CHL, and water depth (Tables 3, 5).

The Neva Estuary is also one of the most eutrophic areas in the Baltic Sea with high phytoplankton biomass in summer (Golubkov et al. 2017, 2021). For this reason, the concentration of chlorophyll was one of the predictors of the euphotic zone depth in the Neva Estuary according to mixed-effects regression analysis (Table 5). Similar results were obtained in the eutrophic Roskilde Estuary within the city of Copenhagen, where the concentration of chlorophyll *a* had the main effect on Kd(PAR), and suspended inanimate organic matter was in second place (Pedersen et al. 2014). There is also an opinion that the depth of the euphotic zone in the coastal areas of the Baltic Sea is mainly affected by inorganic suspended matter (Lund-Hansen 2004; Kratzer and Tett 2009; Kari et al. 2018), while in open waters, it depends on the concentration of CDOM and phytoplankton during algal blooms (Neumann et al. 2015; Harvey et al. 2019). However, in the Neva Estuary, the depth of the euphotic zone depended on both the concentration of mineral suspended matter and phytoplankton (Tables 3, 5). These examples show that there are regional features of the relationship between the euphotic zone depth and various environmental factors.

The formula (2) obtained by us for the relationship between the depth of the euphotic zone and the PAR attenuation coefficient gives a better determination coefficient and very close to formula $4.6/Kd(PAR)$, which was proposed by Kirk (2011) to inland and some turbid coastal waters. This regional formula (2) as well as mixed-effects regression (Table 5) can be used to interpret satellite images of the studied coastal area. Previously, a statistically significant relationship has been shown between Kd(PAR) and the coefficient of vertical attenuation at 490 nm (Kd(490)), which can be easily obtained from satellite images of the Baltic Sea (Mueller 2000; Pierson et al. 2008). Through modeling, Pierson with colleagues (2008) showed that Kd(490) is significantly related not only to Kd(PAR) but also to the depth of the euphotic zone. For example, water transparency parameters were obtained in some parts of the Baltic Sea, as well as in some lakes located in the Baltic catchment using Kd(490) (Alikas and Kratser 2017). The regional coefficients obtained by us increase the accuracy of determining the depth of the euphotic zone in summer, at least in the Neva Estuary. They can also be used to study water productivity from satellite images, taking into account the relationship between Kd(PAR) and Kd(490).

O’Gorman et al. (2016) calculated that in the rivers of the south-west of Iceland, the efficiency of using the PAR energy incident on the water surface to produce gross primary production was 2.4–5.3%. In the case of the Neva Estuary, the average efficiency of using PAR energy to create gross primary production was inversely proportional to the PAR value (Fig. 7a), averaging about 2%. At the same time, the PP did not depend on the amount of radiation incident on the water surface (Fig. 7b). This means that the PP in the estuary was limited by other environmental factors, which included underwater light conditions and nutrient concentrations.

According to Harvey et al. (2019), predicted wetter climate in Scandinavia and, as a result, a future increase in river runoff will lead to a decrease in the euphotic zone due to an increase in the runoff of humic substances from the watershed, which, in turn, may lead to a decrease in the primary production of plankton in coastal waters. For example, it has been shown that CDOM, even at low concentrations, reduces transparency and, as a result, limits primary production in Norwegian lakes, but the lack of light can be compensated by a higher level of nutrients (Thrane et al. 2014). However, a significant increase in precipitation in the region of the Neva Estuary in recent years as a result of changes in atmospheric circulation did not lead to a decrease in primary production in the estuary (Golubkov and Golubkov 2020, 2021). This is apparently due to the fact that, as shown by our studies (Table 3), CDOM did not have a significant effect on the light conditions in the upper and middle reaches of the Neva Estuary. On the contrary, rainy and windy weather observed in the region in 2010s

during the period of the positive anomaly of the North Atlantic Oscillation positively correlated with the concentration of nutrients, chlorophyll, and the primary production of plankton in these parts of the estuary (Golubkov and Golubkov 2020, 2021). It should also be taken into account that high solar insolation and an increase in the intensity of photosynthesis and phytoplankton biomass lead to a rapid depletion of nutrients and a deterioration in light conditions in the water column (Fogel et al. 1992; Fry 1996; Golubkov et al. 2020), which can disguise the effect of an increased CDOM concentration.

In conclusion, one should agree with Harvey et al. (2019) that light conditions in different regions of the Baltic Sea, while seemingly identical, can be determined by different factors, and that more research should be carried out in different water areas to clarify this issue.

Supplementary Information The online version contains supplementary material available at <https://doi.org/10.1007/s12237-022-01164-9>.

Acknowledgements The authors thank the two reviewers for their constructive comments that significantly improved the early version of the manuscript.

Author Contribution All authors drafted, contributed to, and approved the manuscript.

Funding The study was supported by Zoological Institute RAS (project 122031100274–7).

Data Availability Original data available upon request and will be provided immediately.

References

- Alikas, K., and S. Kratzer. 2017. Improved retrieval of Secchi depth for optically-complex waters using remote sensing data. *Ecological Indicators*. <https://doi.org/10.1016/j.ecolind.2017.02.007>.
- Armengol, J., L. Caputo, M. Comerma, C. Feijóo, J.C. García, R. Marcé, E. Navarro, and J. Ordoñez. 2003. Sau reservoir's light climate: relationships between Secchi depth and light extinction coefficient. *Limnética*. [http://refhub.elsevier.com/S0048-9697\(21\)00223-0/rf0005](http://refhub.elsevier.com/S0048-9697(21)00223-0/rf0005).
- Arst, H. 2003. *Optical Properties and Remote Sensing of Multicomponental Water Bodies*. Berlin: Springer-Verlag.
- Arst, H., T. Nöges, P. Nöges, and B. Paavel. 2008. Relations of phytoplankton in situ primary production, chlorophyll concentration and underwater irradiance in turbid lakes. *Hydrobiologia*. <https://doi.org/10.1007/s10750-007-9213-z>.
- Bates, D., M. Mächler, B. Bolker, and S. Walker. 2015. Fitting linear mixed-effects models using lme4. *Journal of Statistical Software*. <https://doi.org/10.18637/jss.v067.i01>.
- Barton, K. 2022. MuMIn: multi-model inference. <https://cran.r-project.org/web/packages/MuMIn/index.html>. Accessed 02 Nov 2022.
- Behrenfeld, M.J., and P.G. Falkowski. 1997. A consumer's guide to phytoplankton primary productivity models. *Limnology and Oceanography*. <https://doi.org/10.4319/lo.1997.42.7.1479>.
- Bianchi, T.S. 2007. *Biogeochemistry of estuaries*. Oxford: University Press.
- Bird, S. M., M. S. Fram, and K. L. Crepeau. 2003. Method of analysis by the U.S. Geological Survey California District Sacramento Laboratory—Determination of dissolved organic carbon in water by high temperature catalytic oxidation, method validation, and quality-control practices. In *Open-file report 03–366*. U.S. Geological Survey. Ed. U.S.G. Survey. <http://pubs.usgs.gov/of/2003/of03366/text.html>. Accessed 02 Nov 2022.
- Christian, D., and Y.P. Sheng. 2003. Relative influence of various water quality parameters on light attenuation in Indian River Lagoon. *Estuarine, Coastal and Shelf Science*. [https://doi.org/10.1016/S0272-7714\(03\)00002-7](https://doi.org/10.1016/S0272-7714(03)00002-7).
- Chupakova, A.A., A.V. Chupakov, N.V. Neverova, L.S. Shirokova, and O.S. Pokrovsky. 2018. Photodegradation of river dissolved organic matter and trace metals in the largest European Arctic estuary. *Science of the Total Environment*. <https://doi.org/10.1016/j.scitotenv.2017.12.0>.
- De Wit, H.A., S. Valinia, G.A. Weyhenmeyer, M.N. Futter, P. Kortelainen, K. Austnes, D.O. Hessen, A. Rärke, H. Laudon, and J. Vuorenmaa. 2016. Current browning of surface waters will be further promoted by wetter climate. *Environmental Science & Technology Letters*. <https://doi.org/10.1021/acs.estlett.6b00396>.
- Devlin, M.J., J. Barry, D.K. Mills, R.J. Gowen, J. Foden, D. Siver, and P. Tett. 2008. Relationships between suspended particulate material, light attenuation and Secchi depth in UK marine waters. *Estuarine, Coastal and Shelf Science*. <https://doi.org/10.1016/j.ecss.2008.04.024>.
- Domingues, R.B., T.P. Anselmo, A.B. Barbosa, U. Sommer, and H.M. Galvao. 2011. Light as a driver of phytoplankton growth and production in the freshwater tidal zone of a turbid estuary. *Estuarine, Coastal and Shelf Science*.
- Downing, B.D., B.A. Pellerin, B.A. Bergamaschi, J.F. Saraceno, and T.E.C. Kraus. 2012. Seeing the light: The effects of particles, dissolved materials, and temperature on in situ measurements of DOM fluorescence in rivers and streams. *Limnology and Oceanography Methods*. <https://doi.org/10.4319/lom.2012.10.767>.
- Eilola, K., H.E.M. Meier, and E. Almroth. 2009. On the dynamics of oxygen, phosphorus and cyanobacteria in the Baltic Sea; a model study. *Journal of Marine Systems*. <https://doi.org/10.1016/j.jmarsys.2008.08.009>.
- Emelyanov, E.M. 2003. *Barrier zones in the oceans*. Berlin: Springer-Verlag.
- Fogel, M.L., L.A. Cifuentes, D.J. Velinsky, and J.H. Sharp. 1992. Relationship of carbon availability in estuarine phytoplankton to isotopic composition. *Marine Ecology Progress Series*. 82: 291–300.
- Fry, B. 1996. $^{13}\text{C}/^{12}\text{C}$ fractionation by marine diatoms. *Marine Ecology Progress Series*. 134: 283–294.
- Golubkov, M., and S. Golubkov. 2020. Eutrophication in the Neva Estuary (Baltic Sea): Response to temperature and precipitation patterns. *Marine and Freshwater Research*. <https://doi.org/10.1071/MF18422>.
- Golubkov, M., and S. Golubkov. 2021. Relationships between northern hemisphere teleconnection patterns and phytoplankton productivity in the Neva Estuary (Northeastern Baltic Sea). *Frontiers in Marine Science*. <https://doi.org/10.3389/fmars.2021.735790>.
- Golubkov, M., and S. Golubkov. 2022. Impact of the Construction of New Port Facilities on Primary Production of Plankton in the Neva Estuary (Baltic Sea). *Frontiers in Marine Science*. <https://doi.org/10.3389/fmars.2022.851043>.
- Golubkov, M., V. Nikulina, and S. Golubkov. 2019b. Effects of environmental variables on midsummer dinoflagellate community in the Neva Estuary (Baltic Sea). *Oceanologia*. <https://doi.org/10.1016/J.OCEANO.2018.09.001>.
- Golubkov, M.S., V.N. Nikulina, and S.M. Golubkov. 2021. Species-level associations of phytoplankton with environmental variability in the Neva Estuary (Baltic Sea). *Oceanologia*. <https://doi.org/10.1016/j.oceano.2020.11.002>.
- Golubkov, M.S., V.N. Nikulina, A.V. Tiunov, and S.M. Golubkov. 2020. Stable C and N isotope composition of suspended particulate organic matter in the Neva Estuary: The role of abiotic factors, productivity, and phytoplankton taxonomic composition. *Journal of Marine Science and Engineering*. <https://doi.org/10.3390/jmse8120959>.

- Golubkov, S., M. Golubkov, A. Tiunov, and V. Nikulina. 2017. Long-term changes in primary production and mineralization of organic matter in the Neva Estuary (Baltic Sea). *Journal of Marine Systems*. <https://doi.org/10.1016/j.jmarsys.2016.12.009>.
- Golubkov, S.M., M.S. Golubkov, and A.V. Tiunov. 2019a. Anthropogenic carbon as a basal resource in the benthic food webs in the Neva Estuary (Baltic Sea). *Marine Pollution Bulletin*. <https://doi.org/10.1016/j.marpolbul.2019.06.037>.
- Gomes, A.C., E. Alcântara, T. Rodrigues, and N. Bernardo. 2020. Satellite estimates of euphotic zone and Secchi disk depths in a colored dissolved organic matter-dominated inland water. *Ecological Indicators*. <https://doi.org/10.1016/j.ecolind.2019.105848>.
- Grasshoff, K., M. Ehrhardt, and K. Kremling. 1999. *Methods of Seawater Analysis, 3rd*. Completely revised and Extended. New York: Wiley-VCH.
- Harvey, E.T., J. Walve, A. Andersson, B. Karlson, and S. Kratzer. 2019. The effect of optical properties on Secchi depth and implications for eutrophication management. *Frontiers in Marine Science*. <https://doi.org/10.3389/fmars.2018.00496>.
- International Organization for Standardization (ISO). 2022. Country Codes–ISO 3166. <https://www.iso.org/iso-3166-country-codes.html>. Accessed 14 Jul 2022.
- Jones, R., I. and L. Arvola. 1984. Light penetration and some related characteristics in small forest lakes in Southern Finland. *SIL Proceedings 1922–2010*. <https://doi.org/10.1080/03680770.1983.11897390>
- Kari, E., I. Merkouriadi, J. Walve, M. Leppäranta, and S. Kratzer. 2018. Development of under-ice stratification in Himmerfjärden bay, North-Western Baltic proper, and their effect on the phytoplankton spring bloom. *Journal of Marine Systems*. <https://doi.org/10.1016/j.jmarsys.2018.06.004>.
- Kim, S.-H., C.-S. Yang, and K. Ouchi. 2015. Spatio-temporal patterns of Secchi depth in the waters around the Korean Peninsula using MODIS data. *Estuarine, Coastal and Shelf Science*. <https://doi.org/10.1016/j.ecss.2015.07.003>.
- Kirk, J.T.O. 2011. *Light and Photosynthesis in Aquatic Ecosystems*, 3rd ed. Cambridge: Cambridge University Press.
- Kottek, M., J. Grieser, C. Beck, B. Rudolf, and F. Rubel. 2006. World Map of the Köppen-Geiger climate classification updated. *Meteorologische Zeitschrift*. <https://doi.org/10.1127/0941-2948/2006/0130>.
- Kratzer, S., and G. Moore. 2018. Inherent optical properties of the Baltic Sea in comparison to other seas and oceans. *Remote Sensing*. <https://doi.org/10.3390/rs10030418>.
- Kratzer, S., and P. Tett. 2009. Using bio-optics to investigate the extent of coastal waters: A Swedish case study. *Hydrobiologia*. <https://doi.org/10.1007/s10750-009-9769-x>.
- Kratzer, S., D. Kyryliuk, M. Edman, P. Philipson, and S.W. Lyon. 2019. Synergy of satellite, in situ and modelled data for addressing the scarcity of water quality information for eutrophication assessment and monitoring of Swedish coastal waters. *Remote Sensing*. <https://doi.org/10.3390/rs11172051>.
- Kuznetsova, A., P.B. Brockhoff, and R.H.B. Christensen. 2017. lmerTest package: tests in linear mixed effects models. *Journal of Statistical Software*. <https://doi.org/10.18637/jss.v082.i13>
- Larsen, S., T. Andersen, and D.O. Hessen. 2011. Climate change predicted to cause severe increase of organic carbon in lakes. *Global Change Biology*. <https://doi.org/10.1111/j.1365-2486.2010.02257.x>.
- Lawson, S.E., P.L. Wiberg, K.J. McGlathery, and D.C. Fugate. 2007. Wind driven sediment suspension controls light availability in a shallow coastal lagoon. *Estuaries and Coasts*. <https://doi.org/10.1111/j.1365-2486.2010.02257.x>.
- Lee, Z.P., K.L. Carder, J. Marra, R.G. Steward, and M.J. Perry. 1996. Estimating primary production at depth from remote sensing. *Applied Optics*. <https://doi.org/10.1364/AO.35.000463>.
- LI-COR. 2022. LI-193 Spherical Underwater Quantum Sensor https://www.licor.com/env/products/light/quantum_underwater_sphere. Accessed 09 Nov 2022.
- Lisitzin, A.P. 1999. The continental-ocean boundary as a marginal filter in the world oceans. In *Biogeochemical cycling and sediment ecology*, ed. J.S. Gray, W. Ambrose, and A. Szaniawska, 69–103. Dordrecht: Springer.
- Lund-Hansen, L.C. 2004. Diffuse attenuation coefficients Kd(PAR) at the estuarine North Sea-Baltic Sea transition: Time-series, partitioning, absorption and scattering. *Estuarine, Coastal and Shelf Science*. <https://doi.org/10.1016/j.ecss.2004.05.004>.
- Martyanov, S., and V. Ryabchenko. 2016. Bottom sediment resuspension in the easternmost Gulf of Finland in the Baltic Sea: A case study based on three-dimensional modeling. *Continental Shelf Research*. <https://doi.org/10.1016/j.csr.2016.02.011>.
- McMahon, T.G., R.C.T. Raine, T. Fast, L. Kies, and J.W. Patching. 1992. Phytoplankton biomass, light attenuation and mixing in the Shannon estuary, Ireland. *Journal of the Marine Biological Association of the UK*. <https://doi.org/10.1017/S0025315400059464>.
- Meteoblue. 2022. Climate Zones. <https://content.meteoblue.com/en/meteoscool/general-climate-zones>. Accessed 09 Nov 2022.
- Morel, A., and R.C. Smith. 1974. Relation between total quanta and total energy for aquatic photosynthesis. *Limnology and Oceanography*. <https://doi.org/10.4319/lo.1974.19.4.0591>.
- Mueller, J.L. 2000. SeaWiFS algorithm for the diffuse attenuation coefficient, K(490), using water-leaving radiances at 490 and 555 nm. In *SeaWiFS Postlaunch Calibration and Validation Analyses, Part 3*, eds. S.B. Hooker, and E.R. Firestone, 24–27. Greenbelt: NASA GSFC.
- Neumann, T., H. Siegel, and M. Gerth. 2015. A new radiation model for Baltic Sea ecosystem modelling. *Journal of Marine Systems*. <https://doi.org/10.1016/j.jmarsys.2015.08.001>.
- Nöges, T., ed. 2001. *Lake Peipsi: Meteorology, hydrology, hydrochemistry*. Tartu: Sulemees Publishers.
- O’Gorman, E.J., O.P. Olafsson, B.O.L. Demars, N. Friberg, G. Gudbergsson, E.R. Hannesdottir, M.C. Jackson, L.S. Johansson, O.B. McLaughlin, J.S. Olafsson, G. Woodward, and G.M. Gislason. 2016. Temperature effects on fish production across a natural thermal gradient. *Global Change Biology*. <https://doi.org/10.1111/gcb.13233>.
- Pedersen, T.M., K. Sand-Jensen, S. Markager, and S.L. Nielsen. 2014. Optical changes in a eutrophic estuary during reduced nutrient loadings. *Estuaries and Coasts*. <https://doi.org/10.1007/s12237-013-9732-y>.
- Philips, E.J., T.C. Lynch, and S. Badylak. 1995. Chlorophyll *a*, tripton, color, and light availability in a shallow tropical inner-shelf lagoon, Florida Bay, USA. *Marine Ecology Progress Series*. <https://doi.org/10.3354/meps127223>.
- Pierson, D.C., S. Kratzer, N. Strömbeck, and B. Håkansson. 2008. Relationship between the attenuation of downwelling irradiance at 490 nm with the attenuation of PAR (400 nm–700 nm) in the Baltic Sea. *Remote Sensing of Environment*. <https://doi.org/10.1016/j.rse.2007.06.009>.
- Riegmann, F., and F. Colijn. 1991. Evaluation of measurements and calculation of primary production in the Dogger Bank area (North Sea) in summer 1988. *Marine Ecology Progress Series* 69: 125–132.
- Ryabchuk, D., V. Zhamoïda, M. Orlova, A. Sergeev, J. Bublischenko, A. Bublischenko, and L. Sukhacheva. 2017. Neva Bay: A technogenic lagoon of the eastern Gulf of Finland (Baltic Sea). In *The diversity of Russian estuaries and lagoons exposed to human influence*, ed. R. Kosyan, 191–221. Cham: Springer International Publishing.
- Savchuk, O.P. 2002. Nutrient biogeochemical cycles in the Gulf of Riga: Scaling up field studies with a mathematical model. *Journal of Marine Systems*. [https://doi.org/10.1016/S0924-7963\(02\)00039-8](https://doi.org/10.1016/S0924-7963(02)00039-8).
- Shirokova, L.S., A.A. Chupakova, A.V. Chupakov, and O.S. Pokrovsky. 2017. Transformation of dissolved organic matter and related trace elements in the mouth zone of the largest European Arctic river:

- Experimental modeling. *Inland Waters*. <https://doi.org/10.1080/20442041.2017.1329907>.
- Southgate, D., and J. Durnin. 1970. Calorie conversion factors. An experimental reassessment of the factors used in the calculation of the energy value of human diets. *British Journal of Nutrition*. <https://doi.org/10.1079/BJN19700050>.
- Swift, T.J., J. Perez-Losada, S.G. Schladow, J.E. Reuter, A.D. Jassby, and C.R. Goldman. 2006. Water clarity modeling in Lake Tahoe: Linking suspended matter characteristics to Secchi depth. *Aquatic Sciences*. <https://doi.org/10.1007/s00027-005-0798-x>.
- Team, R., Core. 2022. R: a language and environment for statistical computing. R Foundation for Statistical Computing. <https://www.r-project.org>. Accessed 9 Nov 2022.
- Telesh, I.V., S.M. Golubkov, and A.F. Alimov. 2008. The Neva Estuary ecosystem. In *Ecology of Baltic Coastal Waters*, ed. U. Schiewer, 259–284. Berlin: Springer-Verlag.
- Thrane, J.E., D.O. Hessen, and T. Andersen. 2014. The absorption of light in lakes: Negative impact of dissolved organic carbon on primary productivity. *Ecosystems*. <https://doi.org/10.1007/s10021-014-9776-2>.
- Turner, J.S., P. St-Laurent, M.A.M. Friedrichs, and C.T. Friedrichs. 2021. Effects of reduced shoreline erosion on Chesapeake Bay water clarity. *Science of the Total Environment*. <https://doi.org/10.1016/j.scitotenv.2021.145157>.
- Wang F., A. Umehara, S. Nakai, and W. Nishijima. 2019. Distribution of region-specific background Secchi depth in Tokyo Bay and Ise Bay, Japan. *Ecological Indicators*. <https://doi.org/10.1016/j.ecolind.2018.11.015>.
- Winter B. 2013. Linear models and linear mixed effects models in R with linguistic applications. <http://arxiv.org/pdf/1308.5499.pdf>. Accessed 14 Jul 2022.
- Zhang, M., Y. Zhou, Y. Zhang, K. Shi, C. Jiang, and Y. Zhang. 2020. Attenuation of UVR and PAR in a clear and deep lake: Spatial distribution and affecting factors. *Limnologia*. <https://doi.org/10.1016/j.limno.2020.125798>.

Springer Nature or its licensor (e.g. a society or other partner) holds exclusive rights to this article under a publishing agreement with the author(s) or other rightsholder(s); author self-archiving of the accepted manuscript version of this article is solely governed by the terms of such publishing agreement and applicable law.